

DIRECT NUMERICAL SIMULATION OF HEAT TRANSPORT IN DISPERSED GAS-LIQUID TWO-PHASE FLOW USING A FRONT TRACKING APPROACH

Niels G. DEEN, Martin VAN SINT ANNALAND and J.A.M. KUIPERS

University of Twente, Fac. of Science and Technology, PO Box 217, 7500 AE Enschede, THE NETHERLANDS

ABSTRACT

In this paper a simulation model is presented for the Direct Numerical Simulation (DNS) of heat transport in dispersed gas-liquid two-phase flow using the Front Tracking (FT) approach. Our model extends the FT model developed by van Sint Annaland et al. (2006) to non-isothermal conditions. In FT an unstructured dynamic mesh is used to represent and track the interface explicitly by a number of interconnected marker points. The Lagrangian representation of the interface avoids the necessity to reconstruct the interface from the local distribution of the fractions of the phases and, moreover, allows a direct and accurate calculation of the surface tension force circumventing the (problematic) computation of the interface curvature. The extended model is applied to predict the heat exchange rate between the liquid and a hot wall kept at a fixed temperature. It is found that the wall-to-liquid heat transfer coefficient exhibits a maximum in the vicinity of the bubble that can be attributed to the locally decreased thickness of the thermal boundary layer.

NOMENCLATURE

a	Computational domain in x-direction (m)
C_p	Heat capacity at constant pressure (J/(kg.K))
D	Distribution function (-)
d	Domain size in x-direction (m)
d_e	Equivalent bubble diameter (m)
Eo	Eötvös number (-)
F	Phase indicator function (-)
Fo	Fourier number (-)
H	Size of domain in (vertical) z-direction (m)
M	Morton number (-)
Nu_p	Nusselt number for penetration theory (-)
Nu_w	Nusselt number for wall heat transfer (-)
p	Pressure (N/m ²)
R	Bubble radius (m)
Re	Reynolds number (-)
s	Tangential co-ordinate direction (m)
T	Temperature (K)
t	Time (s)
v_∞	Bubble rise velocity (m/s)
X_d	Dimensionless volume of drift zone (-)
x_i	i th co-ordinate direction (m)
z	z-co-ordinate (m)

Greek letters

α_p	Instantaneous heat transfer coefficient from penetration theory (W/(m ² .K))
------------	---

α_w	Local instantaneous wall heat transfer coefficient (W/(m ² .K))
λ	Thermal conductivity (W/(m.K))
μ	Dynamic viscosity (kg/(m.s))
$\Delta\rho$	Density difference (kg/m ³)
ρ	Density (kg/m ³)
Δs_m	Surface area of element (m ²)
σ	Surface tension (N/m)

Vectors

\vec{F}_σ	Net surface force acting on marker m (N)
\vec{F}_σ	Volumetric surface tension force (N/m ³)
\vec{G}	Vector quantity defining metrics of the interface (m ⁻¹)
\vec{g}	Gravitational acceleration (m/s ²)
\vec{n}_m	Unit normal vector of marker m (-)
\vec{t}_k	Tangent vector shared with neighbouring element k (m)
\vec{u}	Velocity (m/s)
\vec{x}	Position vector (m)
\vec{x}_m	Position vector of marker m (m)

Subscripts and superscripts

g	Gas phase
l	Dispersed (gas) phase
2	Continuous (liquid) phase
k	Index for edge of marker
p	Penetration theory
w	Wall
z	z-direction

Operators

$\partial / \partial t$	Partial time derivative (s ⁻¹)
∇	Gradient operator (m ⁻¹)
∇^2	Gradient operator (m ⁻¹)
$\nabla \cdot$	Divergence operator (m ⁻¹)
T	Transpose of a tensor

INTRODUCTION

Heat transport in conjunction with multiphase flow phenomena is frequently encountered in a variety of industrial processes involving a.o. coating, granulation, drying and synthesis of fuels (Fischer Tropsch) and base chemicals. Very often in bubbly flows the (local) heat exchange rate (i.e. the Nusselt number) between the continuous (liquid) phase and an immersed surface, for example a tube, is required for basic design procedures. This type of information is hard to access experimentally because of experimental difficulties.

To overcome this problem detailed microscopic models can be used to generate closure laws which are needed in coarse-grained simulation models which are used to describe the macroscopic behaviour and as a practical consequence thereof do not resolve all the relevant length and time scales. This multi-scale modelling approach has been used by the authors previously for dense gas-solid flows (van der Hoef et al., 2004, 2006) and for dispersed gas-liquid two-phase flows (van Sint Annaland et al., 2003 and Deen et al., 2004a, 2004b) and can in principle be used for other types of multiphase flow as well.

Our model is based on a combined Front Tracking (FT) approach. Front Tracking methods have been developed and extensively used by Tryggvason and co-workers (Unverdi and Tryggvason, 1992; Esmaeeli and Tryggvason, 1998a, 1998b and Tryggvason et al., 2001) to a wide variety of very complex free surface problems. In FT an unstructured dynamic mesh is used to represent and track the interface explicitly by a number of interconnected marker points. The Lagrangian representation of the interface avoids the necessity to reconstruct the interface from the local distribution of the fractions of the phases and, moreover, allows a direct and accurate calculation of the surface tension force circumventing the (problematic) computation of the interface curvature. An additional advantage of the FT approach is given by the fact that artificial merging of interfaces, as encountered in Lattice Boltzmann (LB) and Volume of Fluid (VoF) models, can be avoided allowing for the study of collective motion of gas bubbles (swarm behaviour) and induced mixing and suspension of the particulate phase. This method, however also possesses a number of disadvantages among which the rather complex implementation in a computer code and problems with volume conservation should be mentioned. These problems can however be overcome as reported by Dijkhuizen et al. (2005a, 2005b). They successfully applied the FT method to the simulations of the traditionally (very) difficult air-water system (Scardovelli and Zaleski, 1999).

The motivation of this work is to develop a method to investigate heat transfer in multiphase flow systems, as this is a relevant topic for the chemical engineering industries. Most work on this topic is based on empirical correlations, while underlying fundamental knowledge of the interplay between multiphase hydrodynamics and heat transfer is largely lacking. A model that describes all relevant details of the flow and heat transfer can be used to provide the desired fundamental knowledge.

The organisation of this paper is as follows: first the description of the model is given followed by a brief description of the numerical solution method.

Subsequently the results are presented and discussed and finally the conclusions are presented.

MODEL DESCRIPTION

For incompressible multi-material flows the Navier-Stokes equations can be combined into a single equation for the fluid velocity \bar{u} in the entire domain of interest taking into account surface tension through a local volumetric surface force \bar{F}_σ accounting for the presence of the dispersed phase. The governing conservation equations for unsteady, incompressible, Newtonian, multi-fluid flows are given by the following expressions:

$$(\nabla \cdot \bar{u}) = 0 \quad (1)$$

$$\frac{\partial}{\partial t}(\rho \bar{u}) + (\nabla \cdot \rho \bar{u} \bar{u}) = -\nabla p + \rho \bar{g} + \nabla \cdot \mu [(\nabla \bar{u}) + (\nabla \bar{u})^T] + \bar{F}_\sigma \quad (2)$$

where the local averaged density ρ and viscosity μ are evaluated from the local distribution of the phase indicator or colour function function F which is governed by the Poisson equation given below (Unverdi and Tryggvason, 1992), where the vector quantity \bar{G} contains the information on the spatial distribution of the interface:

$$\nabla^2 F = \nabla \cdot \bar{G} \quad (3)$$

the treatment of which will be discussed in more detail in the following section. For the local average density ρ linear weighing of the densities of the continuous (1) and dispersed phase (2) is used:

$$\rho = F \rho_1 + (1 - F) \rho_2 \quad (4)$$

Similarly, the local average dynamic viscosity can also be obtained via linear averaging of the dynamic viscosities of the continuous (1) and dispersed phase (2). As an alternative, more fundamental approach recently proposed by Prosperetti (2001), the local average viscosity can be calculated via harmonic averaging of the kinematic viscosities of the involved phases according to the following expression:

$$\frac{\rho}{\mu} = F \frac{\rho_1}{\mu_1} + (1 - F) \frac{\rho_2}{\mu_2} \quad (5)$$

For certain multi-fluid flows such as parallel flow of two immiscible liquids Eq. 5 offers a better representation of the tangential stress condition at the interface. However, for systems with a high density and viscosity ratio the advantage of using Eq. 5 instead of linear weighing to evaluate the dynamic viscosity is less pronounced. Nevertheless, for all computations reported in this paper Eq. 5 was used to compute the local average viscosity. The thermal energy equation is given by:

$$\rho C_p \left[\frac{\partial T}{\partial t} + (\nabla \cdot \bar{u} T) \right] = (\nabla \cdot \lambda \nabla T) \quad (6)$$

where the volumetric heat capacity ρC_p and the local average conductivity λ are computed respectively from the following equations:

$$\rho C_p = F \rho_1 C_{p,1} + (1-F) \rho_2 C_{p,2} \quad (7)$$

$$\frac{\rho}{\lambda} = F \frac{\rho_1}{\lambda_1} + (1-F) \frac{\rho_2}{\lambda_2} \quad (8)$$

extending respectively Eqs. 4 and 5 to the thermophysical properties.

NUMERICAL SOLUTION METHOD

Computation of the flow and temperature fields

The Navier-Stokes equations are solved with a standard finite volume technique on a staggered rectangular three-dimensional grid using a two-step projection-correction method with an implicit treatment of the pressure gradient and explicit treatment of the convection and diffusion terms. A second order flux delimited Barton-scheme (Centrella and Wilson (1984)) is used for the discretisation of the convection terms and standard second order central finite differences for the diffusion terms. For the thermal energy equation the conduction terms are treated implicitly and the convection terms explicitly. We use a robust and very efficient Incomplete Cholesky Conjugate Gradient (ICCG) algorithm to solve the Pressure Poisson Equation (PPE) and the matrix equation originating from the discretized thermal energy equation.

Computation of the density field

The spatial distribution of the phase indicator function F for both dispersed phases can be obtained from the location of the triangulated interface by solving a Poisson-equation, following the method proposed by Unverdi and Tryggvason (1992):

$$\nabla^2 F = \nabla \cdot \bar{G} = \nabla \cdot \sum_m D(\bar{x} - \bar{x}_m) \bar{n}_m \Delta s_m \quad (9)$$

where the summation is carried out over all surface elements (markers) m representing the interface, using \bar{n}_m to denote the outwardly pointing normal on interface element m and Δs_m its surface area. The function D represents a numerical approximation of the Dirac-

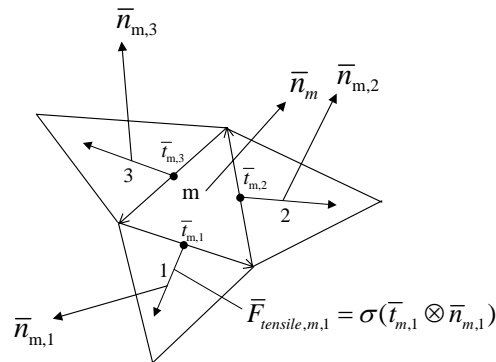


Figure 1: Surface tension force exerted by three neighbouring surface elements on the central surface element.

function normalised to the cell volume. For the distribution function D we typically use volume-weighting, but a distribution function as suggested by Peskin (1977) can be applied as well, however, at the expense of a significantly increased size of the computational stencil.

Computation of the surface force

Following Unverdi and Tryggvason (1992) the surface force acts via a source term \bar{F}_σ in the momentum equation which only acts in the vicinity of the interface. However, our method avoids the explicit computation of the curvature of the interface, but instead uses the following equation as the starting point for the net surface force $\bar{F}_{m,s}$ acting on a single surface element m :

$$\bar{F}_{m,s} = \iint \sigma(\bar{t} \times \bar{n}) ds \quad (10)$$

or its discrete equivalent (see Fig. 1) given by:

$$\bar{F}_{m,s} = \sum_k \sigma(\bar{t}_k \times \bar{n}_k) \quad (11)$$

where \bar{t}_k is the tangent vector (or edge) shared by element m and neighbouring element k and \bar{n}_k its unit normal vector. The summation in Eq. 11 needs to be carried out over all three edges of the element. The tangent vectors can be readily obtained from the known positions of the three corner points of the element. Once the tangent vectors are known the unit normal vector can be easily found from the cross product of two different tangent vectors. Eqs. 10 and 11 give the net surface tension forces acting on a single surface element m and needs, for each separate edge k of the element m , to be distributed to the Eulerian grid to obtain the volumetric surface force appearing in the momentum equation. Since the control volumes for momentum usually contain more than one surface element, the individual element contributions need to be summed. Thus, in our model we compute the volumetric surface force from:

$$\bar{F}_\sigma(\bar{x}) = \frac{\sum_m \sum_k \rho_{m,k} D(\bar{x} - \bar{x}_{m,k}) \sigma(\bar{t}_{m,k} \times \bar{n}_{m,k})}{\sum_m \sum_k \rho_{m,k} D(\bar{x} - \bar{x}_{m,k})} \quad (12)$$

where in addition density weighing is invoked to avoid distribution of the surface force to cells that have a very low liquid volume fraction (Deen et al., 2004b). This treatment of the surface forces produces a stabilising effect on the simulation of systems with a very high density ratio and pronounced surface tension effects (i.e. small air bubbles in water).

Eq. 9 is again solved using standard second order finite difference approximations for the spatial derivatives. The resulting linear equation system is again solved with a robust and very efficient ICCG algorithm. The corner points of the surface elements (markers) are moved with an interpolated velocity field using a simple first order temporal integration method. Since the interface mesh continuously deforms and stretches dynamic remeshing is applied to maintain a proper spatial distribution of the

markers. We use basically the same remeshing procedures

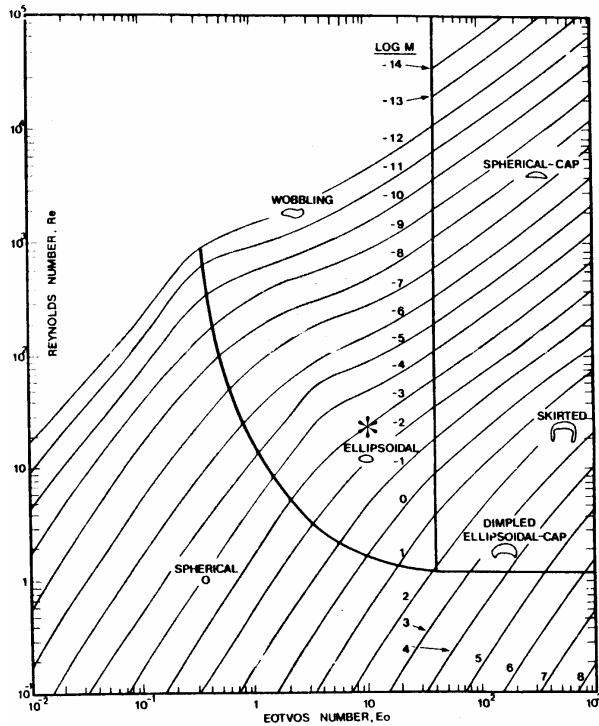


Figure 2: Bubble diagram of Grace (1973) (also see Clift et al., 1978) for the shape and terminal rise velocity of gas bubbles in quiescent viscous liquids.

as reported by Unverdi and Tryggvason (1992) consisting of addition, deletion and reshaping of surface elements. Initially typically 30,000 to 100,000 markers are used to represent the interface of a single bubble.

RESULTS

For a systematic validation of the FT model we refer to van Sint Annaland et al. (2006). They performed extensive calculations for gas bubbles rising in quiescent viscous liquids and demonstrated that the computed terminal rise velocities and shapes of the bubbles agreed very well with those obtained from the Grace diagram (Grace, 1973; Clift et al., 1978) over a very wide range of physical properties, while using a high density and viscosity ratio characteristic for gas-liquid systems. For reference purposes a copy of this diagram, taken from Clift et al. (1978), is reproduced in Fig. 2 where the dimensionless Morton (M), Eötvös (Eo) and Reynolds (Re) numbers are given by:

$$M = \frac{g \mu_1^4 \Delta \rho}{\rho_1^2 \sigma^3} \quad (13)$$

$$Eo = \frac{g \Delta \rho d_e^2}{\sigma} \quad (14)$$

$$Re = \frac{\rho_1 v_\infty d_e}{\mu_1} \quad (15)$$

The equivalent diameter d_e is defined as the diameter of a spherical bubble with the same volume as the bubble

under consideration. In the Reynolds number v_∞ appears which represents the terminal rise velocity of the bubble.

Computational grid	50x50x200 (-)
Grid size	0.0005 m
Time step	0.0001 s
Initial bubble radius	0.005 m
Liquid density	1000 kg/m ³
Liquid viscosity	0.1 kg/(m.s)
Liquid heat capacity	1000 J/(kg.K)
Liquid heat conductivity	10 W/(m.K)
Gas density	10 kg/m ³
Gas viscosity	0.001 kg/(m.s)
Gas heat capacity	1000 J/(kg.K)
Gas heat conductivity	0.025 W/(m.K)
Surface tension	0.1 N/m
Initial gas/liquid temperature	293.0 K
Hot wall temperature	393.0 K

Table 1: Data used for the simulation with hot right wall.

Wall-liquid heat transfer for step change in wall temperature

Here we apply the extended FT-model to predict the heat exchange rate between a liquid and a wall with a step change in the wall temperature. For the simulations (see Table 1 for the data) an initially quiescent liquid phase was assumed with a uniform temperature of 293.0 K. The bubble was released with an initial spherical shape (initial diameter 0.01 m) with its center at one bubble diameter distance from the bottom wall whereas its distance from the hot wall was 0.006 m. In the depth, i.e. the y-direction the bubble was initially positioned in the center. No-slip boundary conditions were imposed at the domain walls. For the thermal energy equation all walls were assumed adiabatic with the exception of the right wall ($x=d=0.025$ m) that was kept at a fixed temperature of 393.0 K.

In Fig. 3 a number of snapshots are given showing the rising bubble together with the computed temperature distribution in the central xz -plane of the column. While the bubble accelerates to its final speed it attains an ellipsoidal shape (as expected on basis of the Grace diagram) and moves away from the wall. The Morton and Eötvös number for this case are respectively approximately equal to 10^{-3} and 10 which, according to the Grace diagram, should correspond with a terminal Reynolds number of 22 (case indicated with an asterisk in Fig. 2) which exceeds the computed Reynolds number of 18. This is to be expected since the width of the computational domain amounts only 2.5 times the (equivalent) bubble diameter. Moreover the bubble moves relatively close to the hot wall which will lead to an additional retardation. Van Sint Annaland et al. (2006) showed that the wall effect becomes negligible small in case the size of the domain is 3 to 4 times larger than the bubble diameter. They also found that the bubble should contain 20 computational cells in each direction to obtain sufficiently accurate results. Since in FT the bubble volume is not intrinsically conserved it was verified that the change in bubble volume was negligible.

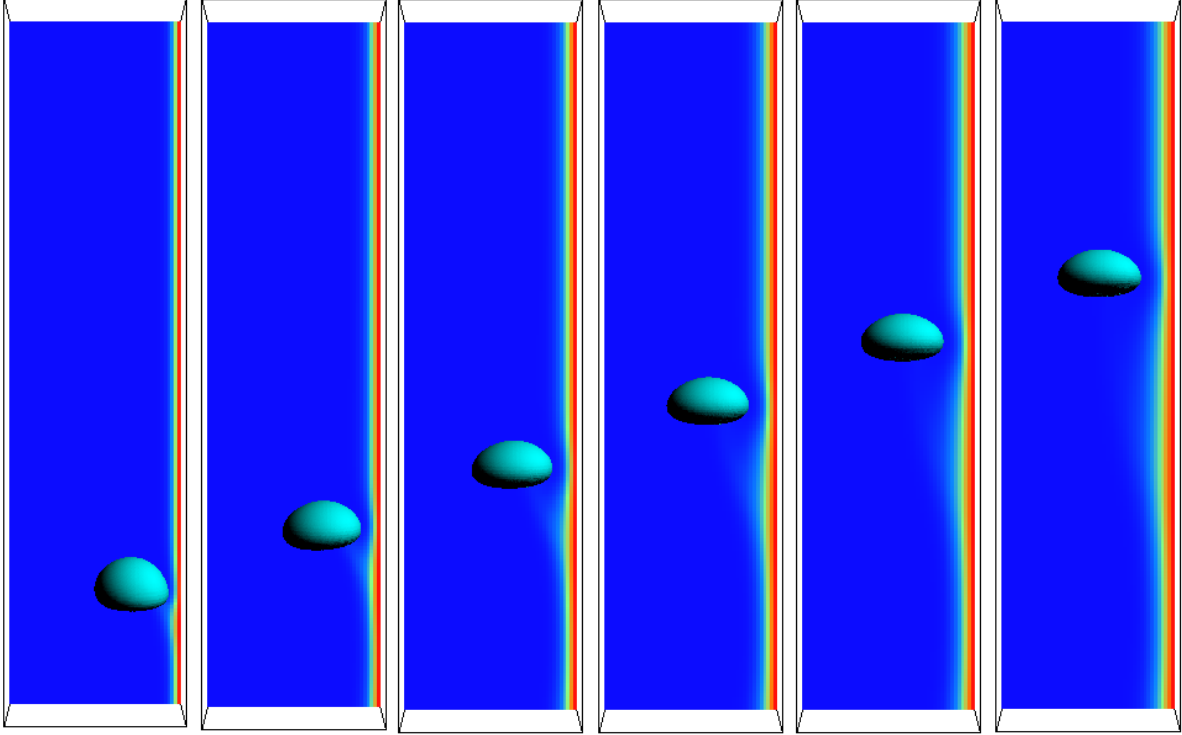


Figure 3: Snapshots at different times of the rise of a gas bubble through an initially quiescent liquid in contact with a hot wall. From left to right: $t=0.05$ s, $t=0.10$ s, $t=0.15$ s, $t=0.20$ s, $t=0.25$ s and $t=0.30$ s after release of the bubble from its initial position ($x=0.0190$ m, $y=0.0125$ m, $z=0.0100$ m). Additional data are given in Table 1.

From the computed temperature distribution the wall-to-liquid heat transfer coefficient was computed and normalized with the instantaneous heat transfer coefficient obtained from the penetration theory:

$$\alpha_p = \sqrt{\frac{\lambda_l \rho_l C_{p,l}}{\pi t}} \quad (16a)$$

The corresponding expression for the Nusselt number Nu_p is given by:

$$Nu_p = \frac{\alpha_p d}{\lambda_l} = \frac{1}{\pi \sqrt{a_l t / d^2}} = \frac{1}{\pi \sqrt{Fo_l}} \quad (16b)$$

where in both expressions (16a) and (16b) the thermophysical properties refer to the (continuous) liquid phase. Typical results are presented in Fig. 4 in terms of the ratio of the Nusselt numbers plotted as function of the vertical (i.e. z) co-ordinate along the wall for the central plane in the depth direction at $t=0.05$ s and $t=0.30$ s after release of the bubble from its initial position. From inspection of this profile we clearly see that the local heat transfer coefficient reaches its maximum at the equator position of the bubble. Below this position the local heat transfer coefficient first decreases and then increases with increasing distance from the bubble. The existence of the maximum at the equator position of the bubble can be explained by the fact that the bubble locally reduces the thickness of the thermal boundary layer leading to a higher heat transfer coefficient. The minimum below the bubble is caused by the heated liquid which flows down between the bubble and the wall. Effectively this leads to an increased thickness of the thermal boundary layer and consequently a decreased local heat transfer coefficient.

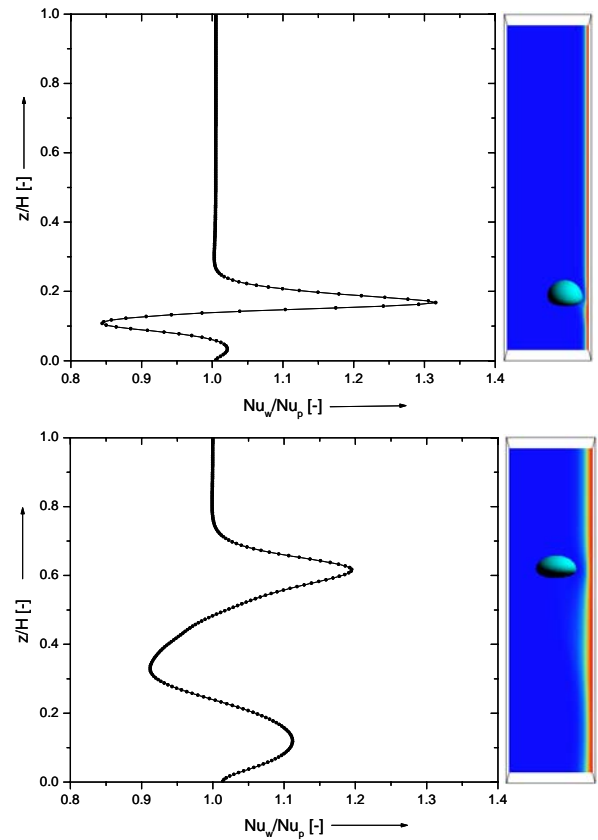


Figure 4: Profile of the instantaneous dimensionless heat transfer coefficient (left) and corresponding bubble position (right) for $t=0.05$ s (top) and $t=0.30$ s (bottom).

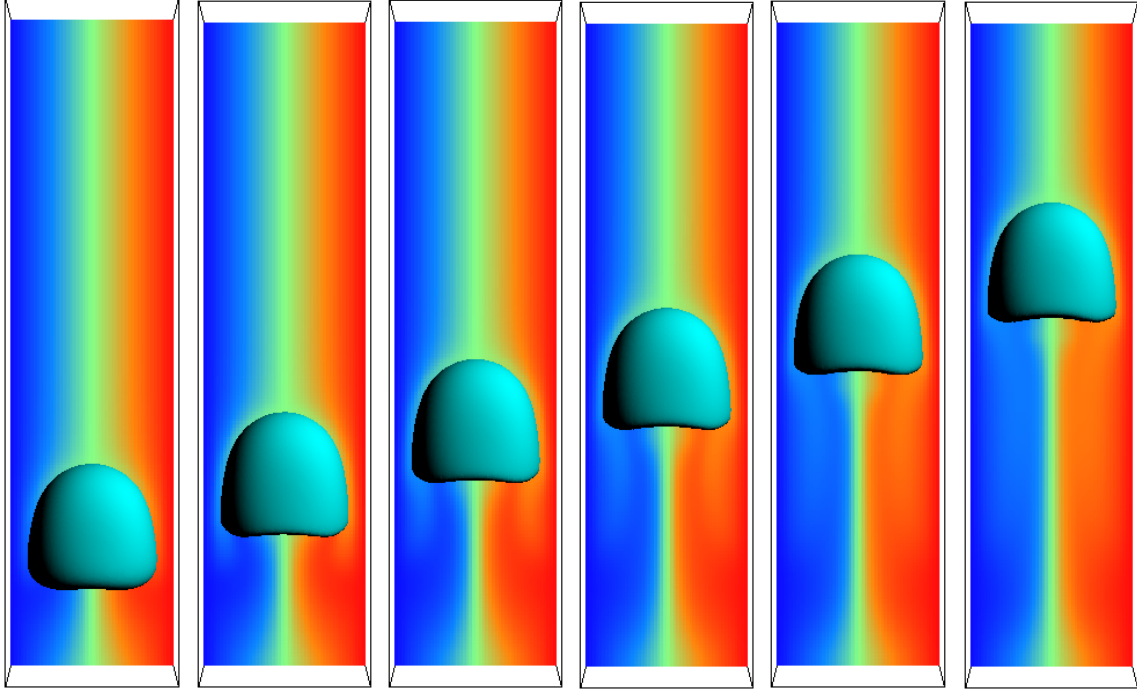


Figure 5: Snapshots at different times of the rise of a gas bubble through an initially quiescent liquid with (initial) linear temperature profile in the x-direction. From left to right: $t=0.05$ s, $t=0.10$ s, $t=0.15$ s, $t=0.20$ s, $t=0.25$ s and $t=0.30$ s after release of the bubble from its initial position ($x=0.0125$ m, $y=0.0125$ m, $z=0.0150$ m). Additional data are given in Table 2.

Wall-liquid heat transfer for equilibrium system

In the first example a system was considered in which a step change in the temperature of one of the confining walls (i.e. $x=d$) was imposed at $t=0$ s. In the second example (see Table 2 for the data) we will consider a system where initially thermal equilibrium prevails and the left and right wall are kept at a temperature of respectively $T_0=293.0$ K and $T_1=393.0$ K whereas in the quiescent liquid a linear temperature profile in the x-direction was taken as the initial condition:

$$T(x) = (T_1 - T_0) \frac{x}{d} + T_0 \quad (17)$$

Computational grid	50x50x200 (-)
Grid size	0.0005 m
Time step	0.0001 s
Initial bubble radius	0.01 m
Liquid density	1000 kg/m ³
Liquid viscosity	0.1 kg/(m.s)
Liquid heat capacity	1000 J/(kg.K)
Liquid heat conductivity	10 W/(m.K)
Gas density	10 kg/m ³
Gas viscosity	0.001 kg/(m.s)
Gas heat capacity	1000 J/(kg.K)
Gas heat conductivity	0.025 W/(m.K)
Surface tension	0.1 N/m
Initial gas/liquid temperature	Linear distribution in x-direction K
Left wall temperature ($x=0$)	293.0 K
Right wall temperature ($x=d$)	393.0 K

Table 2: Data used for the simulation with imposed linear temperature distribution.

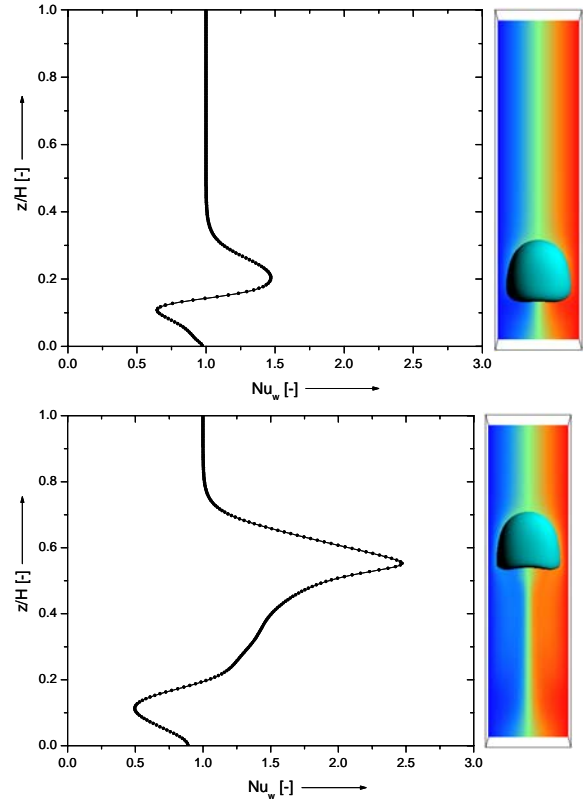


Figure 6: Profile of the instantaneous Nusselt number (left) and corresponding bubble position (right) for $t=0.05$ s (top) and $t=0.30$ s (bottom).

where d is the size of the domain in the x -direction. For this (steady state) system the Nusselt number for the wall-to-liquid heat transfer is given by:

$$Nu_w = \frac{\alpha_w d}{\lambda_l} = 1 \quad (18)$$

The perturbation of the system is created by the rising bubble which is released with an initial spherical shape (initial diameter 0.02 m) in the center of the domain at 0.015 m distance from the bottom wall. No-slip boundary conditions were imposed at the domain walls whereas for the thermal energy equation all walls were assumed adiabatic with the exception of the left ($x=0$) and right wall ($x=d$). In Fig. 5 a number of snapshots are given showing the rising bubble together with the computed temperature distribution in the central xz -plane of the column. Due to the fact that the domain size in the lateral directions only amounts 1.25 times the initial bubble diameter (slug regime), the bubble shape is considerably influenced by the presence of the confining walls. The Morton and Eötvös number for this case are respectively approximately equal to 10^{-3} and 40 which, according to the Grace diagram, should correspond with a terminal Reynolds number of 60 which, as expected, considerably exceeds the computed Reynolds number of 32. Also in this case it was verified that the change in bubble volume was negligible.

In Fig. 6 the instantaneous Nusselt number (defined according to Eq. 18) is plotted as function of the vertical (i.e. z) co-ordinate along the wall for the central plane in the depth direction at $t=0.05$ s and $t=0.30$ s after release of the bubble from its initial position. Similar to the first case a maximum in the heat transfer coefficient is found but now at the base of the bubble where the lateral diameter is at its maximum. Below the bubble the heat transfer coefficient is again relatively low.

CONCLUSIONS

In this paper a simulation model was presented for the Direct Numerical Simulation (DNS) of heat transport in dispersed gas-liquid two-phase flow using the Front Tracking (FT) approach. The FT model developed and validated by van Sint Annaland et al. (2006) was supplemented with a thermal energy equation to extend the model to non-isothermal conditions. The extended model was applied to predict the local heat transfer coefficients between the liquid and a hot wall kept at a fixed temperature. It was found that the profile of the heat transfer coefficient exhibits a maximum in the vicinity of the bubble due to the locally decreased thickness of the thermal boundary layer whereas a region of relatively low heat transfer coefficient exists below the bubble which is attributed to local thermal saturation caused by the downward flowing liquid between the bubble and the hot wall.

REFERENCES

CENTRELLA, J. and WILSON, J. (1984). Planar numerical cosmology. II. The difference equations and numerical tests, *Astrophysical J. Suppl. Ser.* **54**, 229.
CLIFT, R., GRACE, J.R. and WEBER, M. (1978) *Bubbles, Drops and Particles*, Academic Press, New York.

DEEN, N.G., VAN DEN HENGEL, E., VAN SINT ANNALAND, M. and KUIPERS, J.A.M. (2004a) Multi-Scale modelling of dispersed gas-liquid two-phase flow, paper no. K07, CD-ROM proceedings of 5th International Conference on Multiphase Flow, ICMF'04, Yokohama, Japan, May 30-June 4, 2004.

DEEN, N.G., VAN SINT ANNALAND, M. and KUIPERS, J.A.M. (2004b). Multi-level modelling of dispersed gas-liquid two-phase flow, *Chem. Eng. Sci.* **59**, 1853-1861.

DIJKHUIZEN, W., VAN DEN HENGEL, E.I.V., DEEN, N.G., VAN SINT ANNALAND, M. and KUIPERS, J.A.M. (2005a). Numerical investigation of closures for interface forces in dispersed flows using Volume of Fluid and Front Tracking Models, *Chem.Eng.Sci.* **60**, 6169-6175.

DIJKHUIZEN, W., VAN SINT ANNALAND, M. and KUIPERS, J.A.M. (2005b). Numerical investigation of closures for interface forces in dispersed flows using a 3D Front Tracking Model, presented at the Fourth International Conference on CFD in the Oil and Gas, Metallurgical & Process Industries, Trondheim, Norway.

ESMAEELI, A. and TRYGGVASON, G. (1998a), Direct numerical simulation of bubble flows. Part I. Low Reynolds number arrays, *J. Fluid Mech.*, **377**, 313-345.

ESMAEELI, A. and TRYGGVASON, G. (1998b), Direct numerical simulation of bubble flows. Part II. Moderate Reynolds number arrays, *J. Fluid Mech.*, **385**, 325-358.

GRACE, J.R. (1973) Shapes and velocities of bubbles rising in infinite liquids, *Trans. Instn. Chem. Eng.*, **51**, 116-120.

HIRT, C.W. and NICHOLS, B.D. (1981). Volume of Fluid (VOF) method for the dynamics of free boundaries, *J. Comp. Phys.* **39**, 201.

PROSPERETTI, A. (2001), Navier-Stokes numerical algorithms for free-surface flow computations: An overview. *Drop Surface Interactions*, 21.

SCARDOVELLI, S. and ZALESKI, S. (1999). Direct numerical simulation of free-surface and interfacial flow, *Annu. Rev. Fluid Dyn.*, **31**, 567-603.

TRYGGVASSON, G., BUNNER, B. and ESMAEELI, A. (2001). A front tracking method for the computations of multiphase flow, *J. Comp. Phys.*, **169**(2), 708-759.

UNVERDI, S.O. and TRYGGVASON, G. (1992). A front-tracking method for viscous, incompressible multi-fluid flows. *J. Comp. Phys.* **100**, 25-37.

VAN DER HOEF, M.A., VAN SINT ANNALAND, M. and KUIPERS, J.A.M. (2004). Computational fluid dynamics for dense gas-solid fluidized beds: a multi-scale modeling strategy, *Chem. Eng. Sci.*, **59**, 5157-5165.

VAN DER HOEF, M.A., YE, M., VAN SINT ANNALAND, M., ANDREWS, A.T., SUNDARESAN, S. and KUIPERS, J.A.M. (2006). Multi-scale modeling of gas-fluidized beds, *Adv. Chem. Eng.*, **31**, 65.

VAN SINT ANNALAND, M., DEEN, N.G. and KUIPERS, J.A.M. (2003) In: Sommerfeld, M. and Mewes, D. (eds.), *Multi-level modelling of dispersed gas-liquid two-phase flows*, series: Heat and Mass Transfer, Springer, Berlin.

VAN SINT ANNALAND, M., DIJKHUIZEN, W., DEEN, N.G. and KUIPERS, J.A.M. (2006). Numerical simulation of gas bubbles behaviour using a three-dimensional front tracking method, *AIChE J.* **52**, 99-110.